Comparison of Power System Current Sensors via Playback of Electrical Disturbances

Aaron J. Wilson
Oak Ridge National Laboratory
Oak Ridge, TN, U.S.A.
wilsonaj@ornl.gov

Bruce R. J. Warmack
Oak Ridge National Laboratory
Oak Ridge, TN, U.S.A.
warmackrj@ornl.gov

Ryan A. Kerekes
Oak Ridge National Laboratory
Oak Ridge, TN, U.S.A.
kerekesra@ornl.gov

Patrick D. Brukiewa
Oak Ridge National Laboratory
Oak Ridge, TN, U.S.A.
brukiewapd@ornl.gov

***Abstract*—The need to accurately measure high-frequency content in power system voltage and current phenomena is increasingly becoming more of a priority. As the amount of distributed energy resources (DER) and nonlinear loads penetrating the grid increases, so do challenges associated with traditional measurement and metering applications. In this paper, three commercially-available medium-voltage-level current sensors are characterized in terms of their harmonic amplitude and phase performance against reference signals that are "played back" through the sensors through the use of an arbitrary waveform generator. It is shown that none of the three sensors studied are able to faithfully replicate all of the input signals completely, though there are advantages and disadvantages to each in terms of noise, resonance, and induced phase drift. Additionally, the Goodness-of-Fit metric, typically used for PMU model validation, is used to generate side-by-side comparisons of sensor accuracy over a small window around the events under study.**

***Index Terms*—Smart grid, power systems, harmonics, measurement**

I. Introduction

As the power grid expands both in terms of customers and technology, so do the number of complexities associated with protection and metering applications. Increasing numbers of inverter-based resources (IBRs) penetrating the grid lead to a variety of issues that need to be addressed, such as bi-directional power flows and increased harmonics. Thus collection and accurate interpretation of voltage and current harmonic content is rapidly becoming of paramount importance. For this reason, robust sensing technology is needed to ensure a high level of confidence in captured waveforms.

Research is supported by the US Department of Energy (DOE), Office of Electricity, under Contract DE-AC05-00OR22725 with UT-Battelle, LLC, for the US DOE. This manuscript has been authored by UT-Battelle, LLC, under Contract DE-AC05-00OR22725 with the US Department of Energy (DOE). The US government retains and the publisher, by accepting the article for publication, acknowledges that the US government retains a nonexclusive, paid-up, irrevocable, worldwide license to publish or reproduce the published form of this manuscript, or allow others to do so, for US government purposes. DOE will provide public access to these results of federally sponsored research in accordance with the DOE Public Access Plan (http://energy.gov/downloads/doe-public-access-plan).

All electrical sensing equipment possesses some degree of distortive characteristics, due to phenomena such as resonance, temperature, and saturation, among others. Typically, sensors used for protection and metering (such as instrument transformers) are designed to be extremely accurate for steady-state sinusoidal conditions at the fundamental frequency (50 or 60 Hz). Standards such as IEC 61869-2, [1], and IEC 61869-3, [2], for inductive current transformers (CTs) and potential transformers (PTs), for example, provide accuracy limits at the fundamental frequency. These sensor designs present problems for applications monitoring harmonic content, limiting the ability to make accurate decisions based upon the retrieved frequency information. IEC 60044-8 [3], describes accuracy limits for instrument transformers in terms of *ratio* and *phase* errors. While these metrics are typically used for characterization of the effectiveness of the individual transformer effects, the ratio error may be modified into a simple percent error calculation.

Existing literature characterizes sensors in accordance with the ratio and phase errors discussed above, [4]–[8]. Crotti et al. in [4] use a voltage-divider setup along with a National Instruments (NI) PCI Extension for Instrumentation (PXI) data acquisition system to characterize voltage and current transformers as well as their effects on phasor measurement unit (PMU) measurements. In [6], techniques for metrological characterization of CTs and VTs is performed using generated signals at the fundamental frequency plus individual harmonic components.

Cataliotti et al. in [7], perform characterization of clamp-on CT's under non-sinusoidal situations. A compensation method for non-sinusoidal condition-based distortions for CT's and VT's is presented in [5], by using current and voltage harmonics obtained in sinusoidal conditions to "correct" values obtained under non-sinusoidal conditions. In [8], a compensation method based on the "Best Linear Approximation" theory is used to correct for distortions of harmonic signals under non-sinusoidal conditions.

This paper presents a comparison of various electrical

disturbance events - arcing, capacitor switching, and three-phase inrush - and the ways in which three different sensing technologies are able to capture the finer details of the waveforms (i.e. high-frequency content). The experiment utilized a data acquisition-and-playback feature that uses existing data files and plays them through the various sensors via a current amplifier and arbitrary function generator. This paper is not meant to be a recommendation for one sensing technology over another; it is simply presenting observations.

Section II describes the mathematical formulation for the metrics used in analysis. In section III, the experiment is described. Section IV presents results and discussion, and section V concludes the document.

II. Mathematical Formulation for Comparisons

It is necessary to employ metrics that accurately capture the degree of similarities and differences between signals. For that reason, three techniques are discussed next: percent error, phase difference, and goodness-of-fit, [9].

Under steady-state conditions, a distorted current in the power system can be represented by a periodic function consisting of a 60-Hz fundamental wave written I_1 amps and N harmonics, written I_h amps, $h = 2, \dots N$, with the form:

$$i(t) = \sqrt{2}\left[I_1 \sin(\omega t + \phi_1) + \sum_{h=2}^{N} I_h \sin(h\omega t + \phi_h)\right] \quad (1)$$

where $\omega = 2\pi \times 60$ rad/s, and ϕ_h is the phase angle of harmonic h. A sensor measuring the same signal will produce:

$$\hat{i}(t) = \sqrt{2}\left[\hat{I}_1 \sin(\omega t + \hat{\phi}_1) + \sum_{h=2}^{M} \hat{I}_h \sin(h\omega t + \hat{\phi}_h)\right] \quad (2)$$

where ($\hat{}$) indicates estimated parameters, and $M < N$ due to sensor frequency response limitations (e.g. bandwidth and sampling rate). However, this model does not hold for non-steady-state situations.

A. Percent Error

When characterizing sensor performance against the various harmonics, it is beneficial to use the standard percent error formula:

$$e_{ih} = \left|\frac{\hat{I}_h - I_h}{I_h}\right| \times 100\% \quad (3)$$

The expression in (3) describes the percent difference between input current harmonic amplitude I_h and measured current harmonic amplitude $\hat{I}_h$. The percent error formula is a common means of performance evaluation, and encompasses modified versions for gauging performance of instrument transformers, as described by the *ratio error* in [3].

B. Phase Difference

Along with (3), the relative phase displacement between actual and measured harmonic currents $\Delta\phi_{ih}$ may be calculated from [3] as:

$$\Delta\phi_{ih} = \phi_h - \hat{\phi}_h \quad (4)$$

Harmonic amplitudes I_h and $\hat{I}_h$ and phase angles ϕ_h and $\hat{\phi}_h$ are obtained using the Fast Fourier transform (FFT).

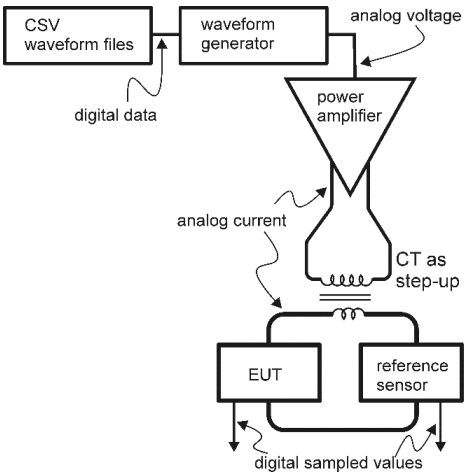

Fig. 1: Experimental setup

C. Goodness-of-Fit (GoF)

Riepnieks and Kirkham in [9] present a metric for evaluating the accuracy of PMUs based on a comparison of the measurement model (the mathematical definition of the quantities being measured) with the observed signal. We have adapted their "goodness-of-fit" (GoF) metric by comparing a time series of measurements recorded from the sensor with that from a reference or ground-truth sensor:

$$GoF = 20\log_{10}\frac{A}{\sqrt{\frac{1}{N-m}\sum_{k=1}^{N}(i_k - \hat{i}_k)^2}}, \quad (5)$$

where A is the amplitude of the signal model, N is the number of points in the time-domain record, m is the number of parameters being measured (in this case, $m = 1$), i_k is the k^{th} sample of the reference time-domain current, and $\hat{i}_k$ is the k^{th} sample of the sensor time-domain current. The GoF is expressed in decibels (dB) in order to ensure the dynamic range is compressed, and the root-mean-square error is in the denominator of (5), yielding greater numbers for closer fits.

III. Experimental Setup and Sensor Description

The basic experimental setup is shown in Fig. 1. Using LabView software, a National Instruments PXIe 6366 Multifunction Data Acquisition System (DAQ) reads comma-separated-value files containing event recordings that are converted to analog waveforms by a NI PXIe 5423 Waveform Generator (WG).

An AE Techron 7228 power amplifier is used to amplify the output function generator voltage and convert to current. The current amplifier was modified to provide a frequency response that is flat to $\pm$ 1% from 60 Hz to $<$ 5 kHz. The current is then stepped up using a KOR-11 15kV 400:5 T200 CT whose frequency response was measured to be flat at least up to 10kHz. On the high side of the step-up transformer, a reference sensor is used to measure the "actual" current being fed into the equipment under test (EUT, i.e. the sensors being evaluated). This is because a phase delay of 20 μs is induced

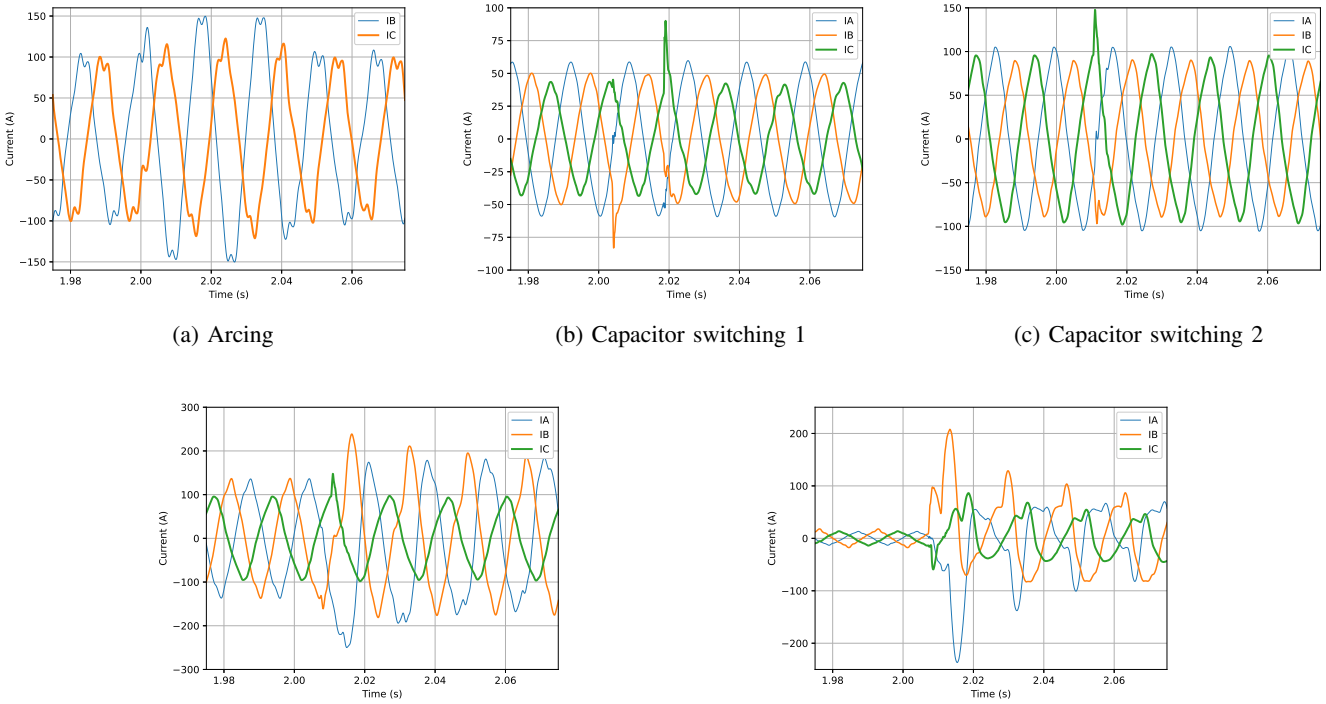

(a) Arcing (b) Capacitor switching 1 (c) Capacitor switching 2

(d) Inrush 1 (e) Inrush 2

Fig. 2: Events used for study

between the EUT signals and WG output signals due to the intermediate equipment.

The Ultrastab 866 Precision Current Transducer (current ratio of 1500:1) was chosen to serve as the reference sensor due to its extremely flat frequency response up to 100 kHz, and is connected to a 10-ohm burden resistor to measure currents of several hundred amps with accuracy better than 0.1 percent. The current signals also pass through the EUT and the measurements are fed back into the DAQ for side-by-side comparison with the reference sensor's readings. Additional current transducers are included in series to provide sanity checks and to calibrate the reference sensor.

The event recordings were sampled at a rate of 256 samples per cycle, or 15,360 Hz. To remain faithful to the original recordings, the DAQ system samples the received reference and EUT signals at the same rate., and synchronizes them. Three sensors were used while conducting the experiments, denoted hereafter as S_1, S_2, and S_3. Each sensor works on a different operating principle, and thus have different eccentricities.

A. Event Descriptions

In total there are 5 events used for study. Each of the 5 events consists of three current phases (A, B, & C) with the exception of one, which only includes phases B & C. Phase A from this particular event did not present any deformities found in the other two phases, so it was discarded.

Fig. 2 shows current-vs.-time plots of the events under study. These events consist of arcing (Fig. 2a), capacitor switching (Figs. 2b-2c), and three-phase inrush (Figs. 2d-2e). All of the noticeable high-frequency contributions appear at the 2-second mark. In Fig. 2a, phase C (orange, thick line) shows a noticeable "blip" at the inception of the arc, whereas phase B (blue, thin line) shows an increase in amplitude for both the fundamental and harmonic components present in the peaks and valleys of the waveform. The capacitor switching events show clear high-frequency content in all three phases, the most extreme of which happen in the "spikes" of phases B (orange, middle-thickness line) and C (green, thick line). Similarly, the inrush events show high-frequency activity on all three phases.

IV. Results and Analysis

Representative plots of sensor performance superimposed upon one another are shown in Fig. 3. In, Fig. 3a, current phase C for the arcing event is shown. It can be seen that sensor S_1 (solid thin line, blue) possesses high-frequency components all along the waveform that are not seen in the reference (dashed, red) waveform. Sensor S_2 appears upon inspection to follow the reference waveform the closest, but it is not without noisy additions as well. Sensor S_3 has trouble responding to instantaneous events and appears to filter out higher harmonics. Figs 3b-3c show example sensor responses to capacitor switching and inrush events, respectively, which contain higher concentrations of harmonic content. S_1 appears to be extremely sensitive to sudden high-frequency changes in

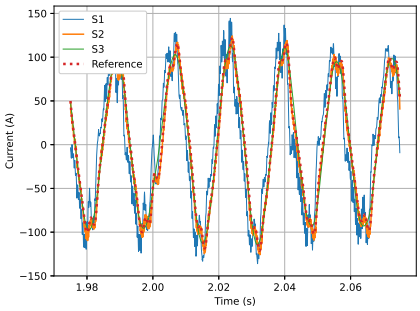

(a) Arcing phase C

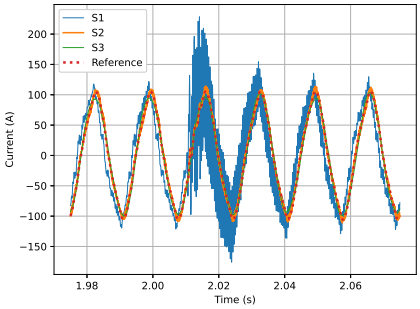

(b) Capacitor switching 2 phase A

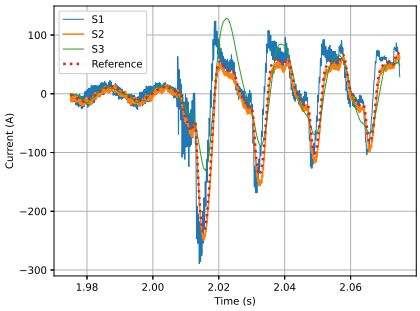

(c) Inrush 2 phase A

Fig. 3: Representative sensor responses

the wave shape. This is due to a very strong resonance in the kHz range.

Tables I-III show amplitude error and phase difference, as computed using (3) and (4), for each of the events shown in Fig. 3. A six-cycle window (0.1 seconds) is used in the FFT calculation, with FFT size equal to 4096 to ensure a small-enough frequency resolution for extracting harmonic amplitudes and phases. Table IV shows the fundamental amplitude errors and phase differences for these events. Additionally, Table IV shows the *mean harmonic errors* and *phase differences* for each event across the 2^{nd} through 35^{th} harmonics.

It is clear from the tables that S_1 presents a significant phase drift across all frequencies and events. S_1 appears to actually *lead* the reference signal during steady-state conditions, for reasons still unknown to the authors. Sensor S_3 performs best

TABLE I: Arcing phase C (AR-IC) harmonic amplitude/phase errors

Parameter	**Harmonic No.**						
	1	3	5	7	11	13	19
S_1 (%)	2.3	30.3	108.4	178,6	70.3	246.3	287.5
S_2 (%)	0.1	2.4	0.1	0.1	0.8	3.1	18.6
S_3 (%)	0.8	42.3	83.4	85.9	40.5	47.2	42.5
S_1 (°)	-22.8	-30.6	-59.2	-64.9	-119	35.7	-111
S_2 (°)	-0.3	-0.5	0.1	0.4	-6.8	-0.1	12.3
S_3 (°)	-1.3	-75.9	130.8	-149.2	16.8	-37.1	2.3

TABLE II: Capacitor switching phase A (CS2-IA) harmonic amplitude/phase errors

Parameter	**Harmonic No.**						
	1	3	5	7	9	11	13
S_1 (%)	2.7	19.7	42.5	78.7	9.5	230.5	135.2
S_2 (%)	0.4	2.1	1.3	1.4	5.8	3.3	3.4
S_3 (%)	0.3	47.1	31.6	21.4	32.5	60.2	16.1
S_1 (°)	-22.8	-36.3	94.6	91	-68.3	-26.6	87.2
S_2 (°)	-0.2	-1	-0.1	0.8	0.3	-1.4	-3.1
S_3 (°)	0.2	18.1	59.3	56.9	54.4	-1.2	48.3

TABLE III: Inrush 2 Phase A (IN2-IA) harmonic amplitude/phase errors

Parameter	**Harmonic No.**						
	1	3	5	7	9	11	13
S_1 (%)	3.8	47.7	100.1	122.6	59.7	132.4	158.1
S_2 (%)	1.8	0.1	5.9	4.6	11.9	5.8	3.8
S_3 (%)	0.6	71.7	75.8	70.9	50.9	64.8	66.4
S_1 (°)	-21.7	-44.3	-48.5	-77.7	-78.3	56.3	-53
S_2 (°)	2.5	1.8	2.6	0.2	2.5	-1.1	108.3
S_3 (°)	1.1	23.1	-1	-119.6	-70.7	-146.8	36.45

under slow-changing (i.e. steady-state) conditions, and does not respond well to sudden changes in amplitude or frequency. S_2 appears to perform the best across the board for all events.

Using the GoF metric defined in (5), each sensor's performance may be characterized as in Fig 4. The y-axis lists each of the events under study, the x-axis is the six-cycle (0.1 second) time window used, and each block represents a single cycle's worth of GoF computed using (5). It is clear from these figures that S_1 performs poorly for the tested events.

S_3 appears to work well for capacitor switching events, but is lackluster for capturing the inrush and arcing events studied. S_2 works best for capturing arcing, inrush event IN1, and the capacitor switching events, but fails to faithfully reproduce the signals contained in IN2. This is likely due to the fact that IN2 has much lower load current levels (15-20 amps as opposed to 100+ amps in the other events), and thus the noise present in the signal is amplified due to the sensor's dynamic range ($<$ 30 kA).

V. Conclusions

The capability for measurement and protection devices to accurately measure the frequency content of a signal is becoming more and more important as smart grid technology advances along with the penetration of distributed energy resources and non-linear loads. This paper has examined the effects of electrical disturbance waveforms with high-

TABLE IV: Fundamental and average harmonic amplitude errors and phase differences for events not shown in Fig. 3

Event	**Fund. (%)** S_1 S_2 S_3	**Fund. (°)** S_1 S_2 S_3	**Mean Harmonic Error (%)** S_1 S_2 S_3	**Mean Harmonic Error (°)** S_1 S_2 S_3
AR-IB	2.7 0.3 1.6	-22.9 -0.4 -1.4	66.8 5.6 11.1	-17.2 3.9 3.3
CS1-IA	3.1 0.4 1.3	-22.9 -0.6 0.3	142.5 8.3 8.1	-26.2 2.2 -0.2
CS1-IB	2.2 0.1 1.4	-23 -0.2 -1.6	524.7 14.5 46.3	-52.1 -3.3 -3.8
CS1-IC	3 1.2 0.8	-23.3 0.8 -1	538.3 14.9 23.4	-51.7 -4.4 21.9
CS2-IB	2.9 0.1 2.4	-23 -0.3 -1.7	631 30.4 37.4	-34.9 0.5 6.7
CS2-IC	3.1 0 0	-22.8 -0.3 -2.9	197.6 7,4 18.2	-15 -0.5 5.1
IN1-IA	3 1.3 2.5	-22.5 -0.3 -1.1	211.7 7.2 68.9	-41.8 -1.1 -18.9
IN1-IB	2.6 0 1.2	-22.8 -0.3 -1.7	72 6 24.3	0.9 0.5 6.1
IN1-IC	3.4 0 0.3	-22.7 -0.3 -2.3	46 23.1 16.9	-24.8 -0.3 0.5
IN2-IB	3.3 0.1 3.9	-23.1 -0.2 -3.1	607.2 15.4 31.5	-58.4 -9.3 18.2
IN2-IC	5.1 0.1 0.5	-22.5 -0.1 -3.3	390.7 11.8 35.5	-48 -4.7 32.8

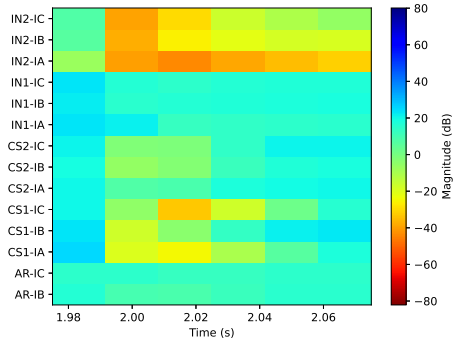

(a) S_1 GoF heatmap

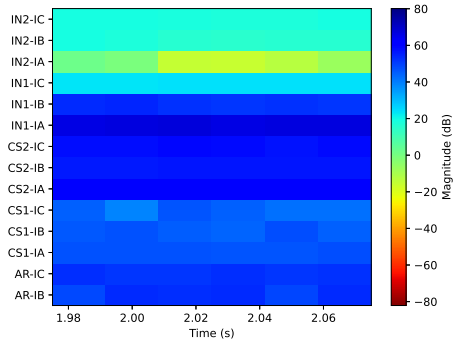

(b) S_2 GoF heatmap

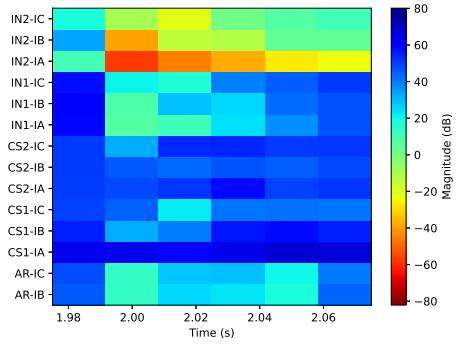

(c) S_3 GoF heatmap

Fig. 4: GoF for each sensor around the event of interest

frequency content as "played back" through three medium-voltage-level sensors. The ability to measure harmonic content is shown to vary considerably across the three sensors. Using the Goodness-of-Fit metric, side-by-side comparisons of each sensor's reproductive capability of high-frequency content reveal variability. It is also shown that none of the sensors out of the three studied are able to perfectly re-create the reference waveforms for all cases. Consequently, knowledge of the harmonic responsiveness of a sensor is essential to understand how it will behave with harmonic-rich disturbances.

ACKNOWLEDGMENT

The authors would like to sincerely thank Texas A&M University for providing Oak Ridge National Laboratory with access to these data sets.

REFERENCES

[1] "Instrument transformers - Part 2: Additional requirements for current transformers," *IEC 61869-2*, 2012.

[2] "Additional requirements for inductive voltage transformers," *IEC 61869-3*, 2011.

[3] "Instrument transformers - Part 8: Electronic current transformers," *IEC 60044-8*, 2002.

[4] G. Crotti, A. D. Femine, D. Gallo, D. Giordano, C. Landi, P. S. Letizia, and M. Luiso, "Traceable characterization of low power voltage instrument transformers for pq and pmu applications," in *2020 Conference on Precision Electromagnetic Measurements (CPEM)*, Conference Proceedings, pp. 1–2.

[5] A. Cataliotti, V. Cosentino, G. Crotti, A. D. Femine, D. D. Cara, D. Gallo, D. Giordano, C. Landi, M. Luiso, M. Modarres, and G. Tin, "Compensation of nonlinearity of voltage and current instrument transformers," *IEEE Transactions on Instrumentation and Measurement*, vol. 68, no. 5, pp. 1322–1332, 2019.

[6] A. Cataliotti, V. Cosentino, G. Crotti, D. Giordano, M. Modarres, D. D. Cara, G. Tin, D. Gallo, C. Landi, and M. Luiso, "Metrological performances of voltage and current instrument transformers in harmonics measurements," in *2018 IEEE International Instrumentation and Measurement Technology Conference (I2MTC)*, Conference Proceedings, pp. 1–6.

[7] A. Cataliotti, D. D. Cara, A. E. Emanuel, and S. Nuccio, "Characterization of clamp-on current transformers under nonsinusoidal conditions," *IEEE Transactions on Power Delivery*, vol. 24, no. 1, pp. 373–380, 2009.

[8] M. Faifer, C. Laurano, R. Ottoboni, S. Toscani, and M. Zanoni, "Characterization of voltage instrument transformers under nonsinusoidal conditions based on the best linear approximation," *IEEE Transactions on Instrumentation and Measurement*, vol. 67, no. 10, pp. 2392–2400, 2018.

[9] A. Riepnieks and H. Kirkham, "An introduction to goodness of fit for pmu parameter estimation," *IEEE Transactions on Power Delivery*, vol. 32, no. 5, pp. 2238–2245, 2017.